Received: 30 April 2021 | Revised: 18 June 2021 | Accepted: 19 June 2021

DOI: 10.1111/jon.12905

JOURNAL OF NEUROIMAGING
THE OFFICIAL JOURNAL OF THE AMERICAN SOCIETY OF NEUROIMAGING
WILEY

CLINICAL INVESTIGATIVE STUDY

Prediction of H3K27M mutation status of diffuse midline gliomas using MRI features

Richa Singh Chauhan[1] | Karthik Kulanthaivelu[1] | Nihar Kathrani[2] | Abhishek Kotwal[1] | Maya Dattatraya Bhat[1] | Jitender Saini[1] | Chandrajit Prasad[1] | Dhritiman Chakrabarti[3] | Vani Santosh[4] | Alok Mohan Uppar[5] | Dwarakanath Srinivas[5]

[1] Department of Neuroimaging and Interventional Radiology, National Institute of Mental Health and Neurosciences (NIMHANS), Bengaluru, India

[2] Consultant Interventionalist, Paras Hospital, Gurugram, India

[3] Department of Neuroanaesthesia and Neuro Critical Care, National Institute of Mental Health and Neurosciences (NIMHANS), Bengaluru, India

[4] Department of Neuropathology, National Institute of Mental Health and Neurosciences (NIMHANS), Bengaluru, India

[5] Department of Neurosurgery, National Institute of Mental Health and Neurosciences (NIMHANS), Bengaluru, India

Correspondence
Maya Dattatraya Bhat, Department of Neuroimaging and Interventional Radiology, National Institute of Mental Health and Neurosciences (NIMHANS), Bengaluru 560029, India.
Email: mayabhat05@yahoo.co.in

Funding information
No funding was received for conducting this study.

Abstract

Background and Purpose: Presurgical prediction of H3K27M mutation in diffuse midline gliomas (DMGs) on MRI is desirable. The purpose of this study is to elaborate conventional MRI (cMRI) features of H3K27M-mutant DMGs and identify features that could discriminate them from wild-type (WT) DMGs.

Methods: CMRI features of 123 patients with DMG were evaluated conforming to the institutional research protocols. Multimodality MRI was performed on 1.5 or 3.0 Tesla MR Scanners with imaging protocol, including T1-weighted (w), T2w, fluid-attenuated inversion recovery, diffusion-weighted, susceptibility-weighted, and postcontrast T1w sequences. Pertinent cMRI features were annotated along the lines of Visually AcceSAble Rembrandt Images features, and Intra Tumoral Susceptibility Signal score (ITSS) was evaluated. R software was used for statistical analysis.

Results: Sixty-one DMGs were H3K27M-mutant (mutant DMGs). The patients in the H3K27M-mutant DMG group were younger compared to the WT-DMG group (mean age 24.13 ± 13.13 years vs. 35.79±18.74 years) ($p = 0.016$). The two groups differed on five cMRI features−−(1) enhancement quality ($p = 0.032$), (2) thickness of enhancing margin ($p = 0.05$), (3) proportion of edema ($p = 0.002$), (4) definition of noncontrast-enhancing tumor (NCET) margin ($p = 0.001$), and (5) cortical invasion ($p = 0.037$). The mutant DMGs showed greater enhancement and greater thickness of enhancing margin, while the WT DMGs exhibited significantly larger edema proportion with poorly defined NCET margins and cortical invasion. ITSS was not significantly different among the groups.

Conclusion: CMRI features like enhancement quality, the thickness of the enhancing margin, proportion of edema, definition of NCET margin, and cortical invasion can discriminate between the H3K27M-mutant and WT DMGs.

KEYWORDS
diffuse midline glioma, H3K27M, MRI, VASARI

INTRODUCTION

Diffuse midline glioma (DMG), H3K27M-mutant, as a distinct set of tumors has been recently categorized in the revised 2016 World Health Organization (WHO) classification of the Central Nervous System (CNS) tumors that exploit an integrated diagnosis combining both histological features and molecular signature. The term assembles diffuse intrinsic pontine gliomas (DIPGs) and infiltrating high-grade glial tumors of the midline carrying the similar canonical mutation at the Lysine 27 residue of the N-terminal tail of histone H3 with its unique recurrent substitution by methionine in the histone H3 variants, H3.3 (approximately 75% cases) and H3.1 (approximately 25% cases). These histone variants are encoded by H3F3A and HIST1H3B/C genes, respectively.[1–3] This observation is in contrast to the hemispheric gliomas, where glycine to arginine substitution occurs in the H3F3A gene (H3G34R). The tumors harboring this mutation have been reported to be high grade that clinically behave aggressively and portend an unfavorable outcome compared to their wild-type (WT) counterparts. Typically, these lesions display a short median survival duration of approximately 9–11 months from the time of diagnosis regardless of the site of the tumor. They have, therefore, been designated by WHO as grade IV tumors irrespective of their histologic morphology.[3,4] Primary childhood brain neoplasms are rare lesions, with an incidence of ~2200 cases per year and DIPG makes up ~20% of these tumors.[5] Being a rare class of tumors, the exact incidence of DMGs harboring H3K27M mutation is still relatively unknown.[6]

As opposed to the previous terminology of DIPG, the term "DMG" specifies that these lesions are not solely centered in the pons/brainstem but may also originate in the other midline structures like thalami, gangliocapsular region, cerebellum, cerebellar peduncles, third ventricle, hypothalamus, and the pineal region as well as in the spinal cord.[2,7–9] Being a rare class of tumors, the exact incidence of DMGs harboring H3K27M mutation (mutant DMGs) remains uncertain. While historically recognized as a pediatric predilection, mutant DMGs can occur across all age groups.[6,10] Diffuse brainstem gliomas are, in general, more aggressive in the pediatric age group than in adults.[2] In children harboring mutant DMGs, the median survival of less than 12, with less than 10% 2-year survival rate, while some of the series of adult patients have shown variable median survival rates of up to 20 months.[5,6]

The critical anatomical location and the infiltrative nature of the tumor in the thalamus or brainstem limit any meaningful surgical resection, and treatment usually employed is fractionated radiotherapy (RT). Multiple monotherapies and combination chemotherapy regimens have also been tried with equivalently dismal outcomes.[5] Despite RT and chemotherapy, DMG in children had a poor prognosis as a 2-year overall survival rate of less than 10%.[11] Since the tumor involves eloquent areas of the brain, a biopsy is usually avoided, and diagnosis of DMGs hinges on clinical and imaging features.[7,10] Imaging modalities like CT and MRI aid in localization, diagnosis, guiding treatment, and dynamically/temporally monitoring the disease evolution and response to treatment. Conventional MRI (cMRI) is commonly used for brain tumor evaluation. The Visually AcceSAble Rembrandt Images (VASARI) MRI feature set has been designed to facilitate reliable depictions of gliomas through organized terminology and distinct visual imaging features. It is given by The Cancer Imaging Archive.[12] The use of the VASARI feature set has been adopted earlier for the molecular subtyping of gliomas and to predict isocitrate dehydrogenase mutation status.[13,14] DMGs are frequently diagnosed based on CT or MRI features as part of these patients' initial evaluation. To the best of our knowledge, there are very few studies that have reported the use of conventional MRI features to differentiate the H3K27M mutant DMGs from WT DMGs. Further, none of the previous reports have utilized an extensive set of conventional imaging features used in the VASARI feature set for the distinction of mutational status in the DMGs.

Therefore, we studied the demographic, clinical, pathological, and imaging features of DMG patients retrospectively. We adopted imaging features similar to those described in VASARI but relevant to midline gliomas for annotating these tumors on MRI. Our study aimed at assessing the cMRI markers to predict the H3K27M mutation status in DMGs noninvasively.

METHODS

This was a retrospective observational study performed at a tertiary referral center conforming to the institutional research protocols. Informed consent was obtained from each patient. We searched our hospital's database retrospectively for the gliomas involving various midline structures of the brain, including the septal region, hypothalamus, thalamus brainstem, cerebellum, middle cerebellar peduncles, and pineal region from June 2016 to April 2020.

Patient cohort

The cases included in the study had (1) MRI suggestive of DMG, (2) who had not received any therapy or had not undergone biopsy or surgical resection before the MRI examination, and (3) for whom the histopathology and immunohistochemistry (IHC) reports were available. All the patients underwent stereotactic biopsy or surgical resection within 1 month of the MRI. The exclusion criteria were: (1) patients with cerebral hemispheric mass lesions; (2) patients with spinal cord lesions; (3) those subjects where imaging or Histopathological Examination (HPE) was suggestive of WHO grade I pilocytic astrocytomas or tumor subtypes other than glioma; (4) inconclusive biopsy; (5) biopsy-proven DMGs with no MRI study; and (6) IHC for H3K27M mutation status unavailable. A total of 123 consecutive cases fulfilled the inclusion criteria and were finally enrolled in the study, of which 61 patients had mutant DMGs (age [years] = 24.13±13.13), and 62 patients had WT DMGs (age = 35.79±18.74) (Figure 1).

Histopathology and immunohistochemistry

Ninety-seven of 123 patients underwent surgical resection, and 26 patients underwent stereotactic biopsy. All the tumors were reviewed by the neuropathologist and were histologically categorized as

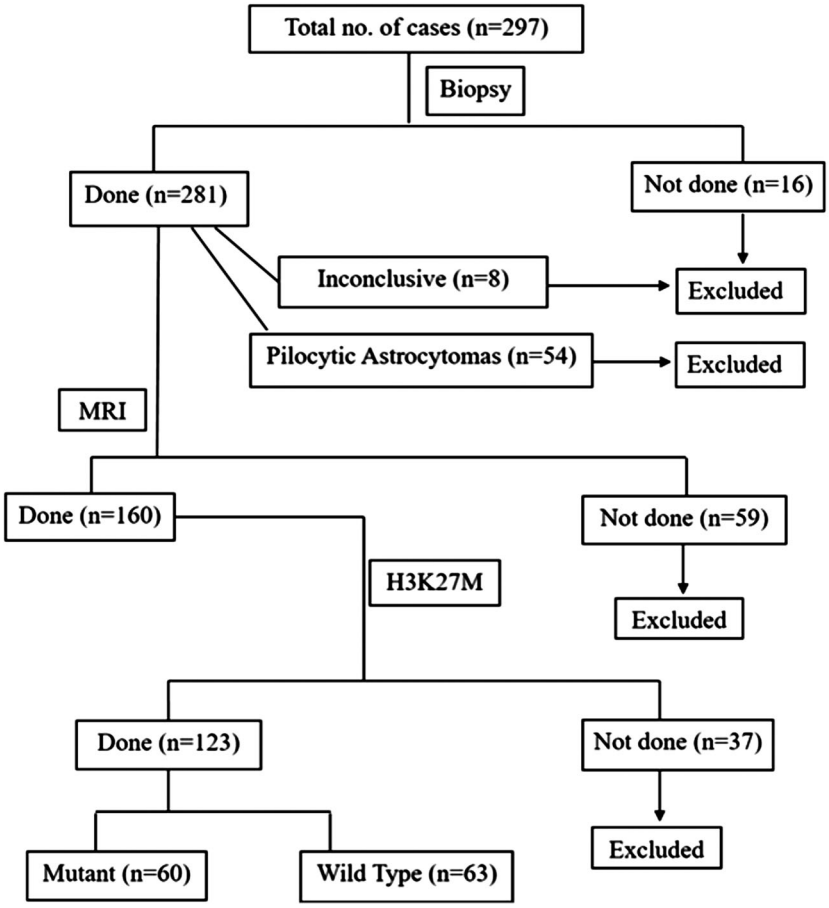

FIGURE 1 Inclusion and exclusion criteria. Flow chart depicting the cases included in the study. Abbreviation: *n*, number of patients

phenotypic low-grade diffuse astrocytomas (grade II), anaplastic astrocytomas (grade III), glioblastomas (grade IV), and DMGs (grade IV). For IHC, formalin-fixed paraffin-embedded sections (4 μm) from the blocks were collected on silane-coated slides. IHC was performed using the Ventana Benchmark automated staining system (Ventana Benchmark-XT). Briefly, the sections were subjected to antigen retrieval followed by incubation with primary and then secondary antibodies. Counterstaining was done with hematoxylin. The antibodies used were as follows: H3K27me3 (Millipore, 07–449; 1:100) (H3.3K27Mme3, Malaysia, RM192, 1:100); Anti-mIDH1 R132H (dilution 1:50, internal clone H06, Dianova, Hamburg, Germany); Sigma polyclonal anti ATRX antibody in 1:100 dilutions; and DAKO P53 antibody in 1:200 dilutions, D07 clone. Appropriate positive or negative controls were included in each batch of staining. The neuroradiologists were blinded to the pathology results of the cases.

TABLE 1 Demographic data and location

	All patients ($n = 123$)	H3K27M Mutant ($n = 61$)	H3K27M WT ($n = 62$)
Age range (in years) Mean ± SD	2–72 30.01 ± 17.16	3–55 24.13 ± 13.13	2–72 35.79 ± 18.74
Gender Male Female	61 62	28 33	33 29
Location (*n* [%])			
Thalamus	79 (64)	36 (59)	43 (69)
Midbrain	10 (8)	8 (13)	2 (3)
Pons	17 (14)	13 (21)	4 (6)
Medulla	3 (3)	2 (3)	1 (2)
Others	14 (11)	2 (3)	12 (20)

Note: Patients' demographic data and location of the mutant and wild-type (WT) diffuse midline gliomas.
Abbreviations: *n*, number of patients; SD, standard deviation.

Image acquisition

MRI was performed on the 1.5 (Aera 1.5 T, Siemens Medical Systems, Erlangen, Germany) or 3.0 (Achieva 3T, Philips Medical Systems, Best, Netherlands) Tesla MR Scanners using 32 channel head coil as per standard operating procedure with/without sedation. MRI protocol included the following sequences: T2-weighted Turbo spin-echo axial and coronal (Repetition Time [TR]/Echo Time [TE]: 3000–4900/80–99 ms), T1-weighted spin-echo axial (TR/TE: 500–600/10 ms), fluid-attenuated inversion recovery (FLAIR) (TR/TE: 9000–11,000/87–125 ms, IR delay 2500–28,003 ms), and susceptibility-weighted imaging (SWI)/Venobold (TR/TE: 31–49/7.2–30 ms), before contrast administration with 512×512 matrix size, 5 mm slice thickness, and 1 mm interslice gap. Postcontrast 3D T1 magnetization prepared rapid gradient echo sequence was acquired after intravenous administration of gadolinium-based contrast agent (Gadovist [Gadobutrol] 0.1 mmol/kg): (256×256) matrix size, 1×1×1 mm^3 in-plane resolution, TR/TE = 6.7/3 ms (3T) and 2200/2.6 ms (1.5T). Intra Tumoral Susceptibility Signal (ITSS) scoring was also done on the Venobold and SWI images.

Qualitative imaging features

All the MRI scans were reviewed on the picture archiving and communication system by two independent neuroradiologists. Our analysis adopted the broad range of imaging attributes as laid out in the VASARI dataset for a detailed characterization of the lesions on conventional MRI. The following parameters were evaluated: tumor location, side of lesion center, involvement of the eloquent brain, enhancement quality (defined as the degree of contrast enhancement in parts of the lesion with postcontrast T1 W sequence; categorized subjectively as mild/minimal = where the degree of enhancement is barely discernible and marked/avid = where the degree of tissue enhancement is intense and obvious; f4 VASARI), proportion contrast-enhancing tumor (CET), proportion noncontrast-enhancing tumor (NCET), proportion necrosis, cysts, multifocal or multicentric or gliomatosis pattern, T1/FLAIR ratio, the thickness of enhancing margin (maximum thickness), the definition of the enhancing margin, the definition of the nonenhancing margin, proportion of edema, hemorrhage, pial invasion, ependymal extension, cortical involvement, deep white matter invasion, NCET crosses the midline, CET crosses midline, and the presence of satellites lesions as per the definition.[12] Few parameters like overall tumor margin and presence of exophytic component, hydrocephalus, and mass effect were also evaluated other than the VASARI feature set.

ITSS scoring was also performed as specified by Park et al.[15] ITSS was defined as low signal tubular or dot-like structures with or without conglomeration within the tumor in high-resolution SWI. ITSS was divided into four grades: grade 0 (no ITSS); grade 1 (1–5 dot-like or tubular ITSS); grade 2 (6–10 dot-like or tubular ITSS), and grade 3 (> 11 dot-like or tubular ITSS).

Intergroup analysis of various features was done between overall mutant and WT DMGs irrespective of tumor grade and location. Furthermore, subgroup analysis for thalamic, brainstem, and grade IV mutant and WT DMGs was also performed.

Statistical analysis

Data were collated offline in a Microsoft Excel 2007 spreadsheet in a deidentified manner. The analysis was conducted using R software version 3.5.2. Interval-scale data were presented as means and standard deviations, and nominal-scale data are presented as frequencies and percentages. Between-group analysis of interval-scale data was conducted using the nonparametric Mann–Whitney U test. Normality of within-group data was observed qualitatively using histograms, and for conformity of analysis, nonparametric methods were chosen. Between-group analysis of nominal-scale data was conducted using a Chi-square test with or without Yate's correction as appropriate. A p-value of < 0.05 was considered statistically significant.

RESULTS

Sixty-one out of 123 cases (49.59%) harbored H3K27M mutation, while 62 patients (50.41%) had H3K27M WT status. The mean age of patients in the mutant DMG group was 24.13 ± 13.13 years, while in the WT group was 35.79 ± 18.74 years ($p = 0.016$). There were 62 female and 61 male patients, and gender distribution was not significantly different between the two groups. Mutant DMGs were graded as WHO grade IV tumors owing to positive H3K27M mutation status. Six (10%) out of 62 WT DMGs were diffuse astrocytomas (grade II), 31 (50%) were anaplastic astrocytomas (grade III), and 25 (40%) were glioblastomas (grade IV).

In our study, the thalamus was the most favored site (64%), followed by the brainstem (25%) and other locations (11%). Fifty-nine percent ($n = 36$) of the 61 H3K27M mutant tumors were located in the thalamus, 38% ($n = 23$) in the brainstem (13%, 21%, and 3% in the midbrain, pons, and medulla, respectively), and the remaining 3% ($n = 2$) were centered in the other locations (one each in the pineal region and cerebellum). Out of the 62 WT DMGs, 69% ($n = 43$) had epicenters in the thalamus, 11% ($n = 7$) in the brainstem (3%, 6%, and 2% in the midbrain, pons, and medulla, respectively), and the rest 20% ($n = 12$) were located elsewhere; 3 (5%) in septal region, 1 (2%) in the pineal region, 6 (9%) in middle cerebellar peduncles, and 2 (3%) in the cerebellum (Table 1). There was no statistically significant difference between the two groups based on the thalamic location ($p = 0.313$). However, the higher frequency of the brainstem location of mutant DMGs was significant ($p = 0.0014$).

On intergroup analysis between the mutant and WT DMGs, five of the studied conventional imaging features evaluated showed significant differences. These features were the (1) enhancement quality ($p = 0.032$); (2) the thickness of the enhancing margin ($p = 0.05$); (3)

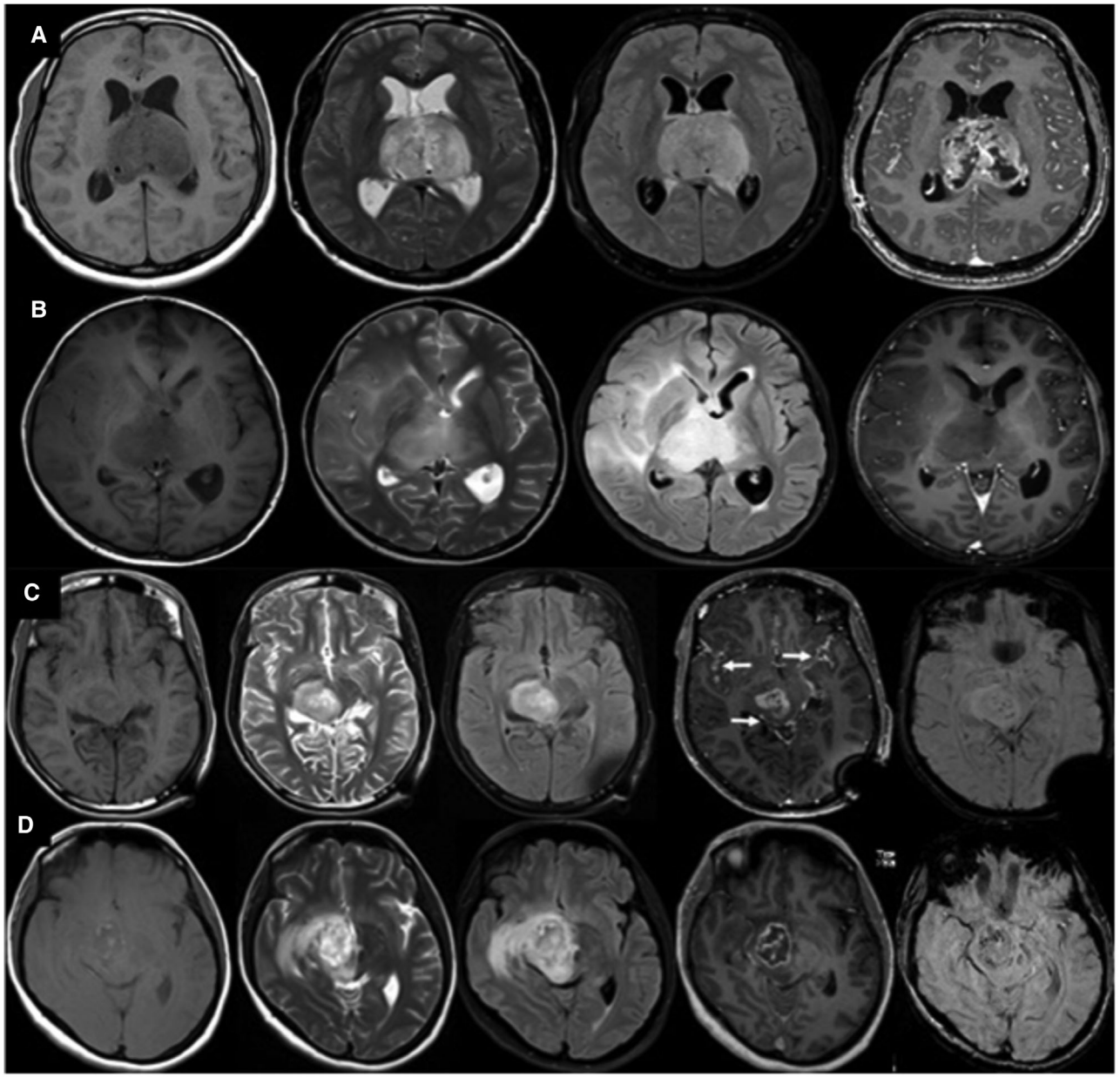

FIGURE 2 Examples of H3K27M-mutant and wild-type bithalamic (A and B) and midbrain (C and D) diffuse midline gliomas (DMGs). A 24-year male patient with H3K27M-mutant DMG (A, first row) shows a well-marginated, heterogeneous bithalamic lesion with no associated edema, intense post contrast enhancement with thick enhancing margins. A 9-year male child with H3K27M wild-type DMG (B, second row) shows a homogeneous bithalamic tumor with extensive edema in right cerebral hemisphere, poorly marginated noncontrast-enhancing tumor, and no post contrast enhancement. A 17-year male with H3K27M-mutant (C, third row) DMG shows a heterogeneous lesion without perilesional edema, solid enhancement with well-marginated noncontrast-enhancing tumor. There is pial extension of the lesion with leptomeningeal enhancement along the ambient cistern and bilateral sylvian fissures (arrows). Note that the lesion shows Intra Tumoral Susceptibility Signal score (ITSS) of 3. A 45-year male with H3K27M wild-type DMG (D, last row) shows a heterogeneous lesion with associated perilesional edema, poor margins of the noncontrast-enhancing tumor, and thin rim enhancement. Note the intralesional ITSS of 3

proportion of edema ($p = 0.002$); (4) definition of NCET margin ($p = 0.001$); and (v) cortical invasion ($p = 0.037$). The mutant DMGs showed significantly greater enhancement as well as the greater thickness of enhancing margin or solid enhancement. The WT DMGs exhibited a significantly larger proportion of edema with a poorly defined NCET margin and a larger degree of cortical invasion compared with the mutant DMGs (Figures 2–4). Few other parameters like tumor heterogeneity ($p = 0.07$), overall tumor margin ($p = 0.074$), and definition of CET margin ($p = 0.073$) tend to approach the level of significance with a higher trend of heterogeneity in the mutant group, and WT tumors were showing more ill-defined margins (Table 2).

On subgroup analysis, an additional feature of the presence of exophytic component showed a significant difference with mutant thalamic gliomas (52.78%) showing more exophytic components as

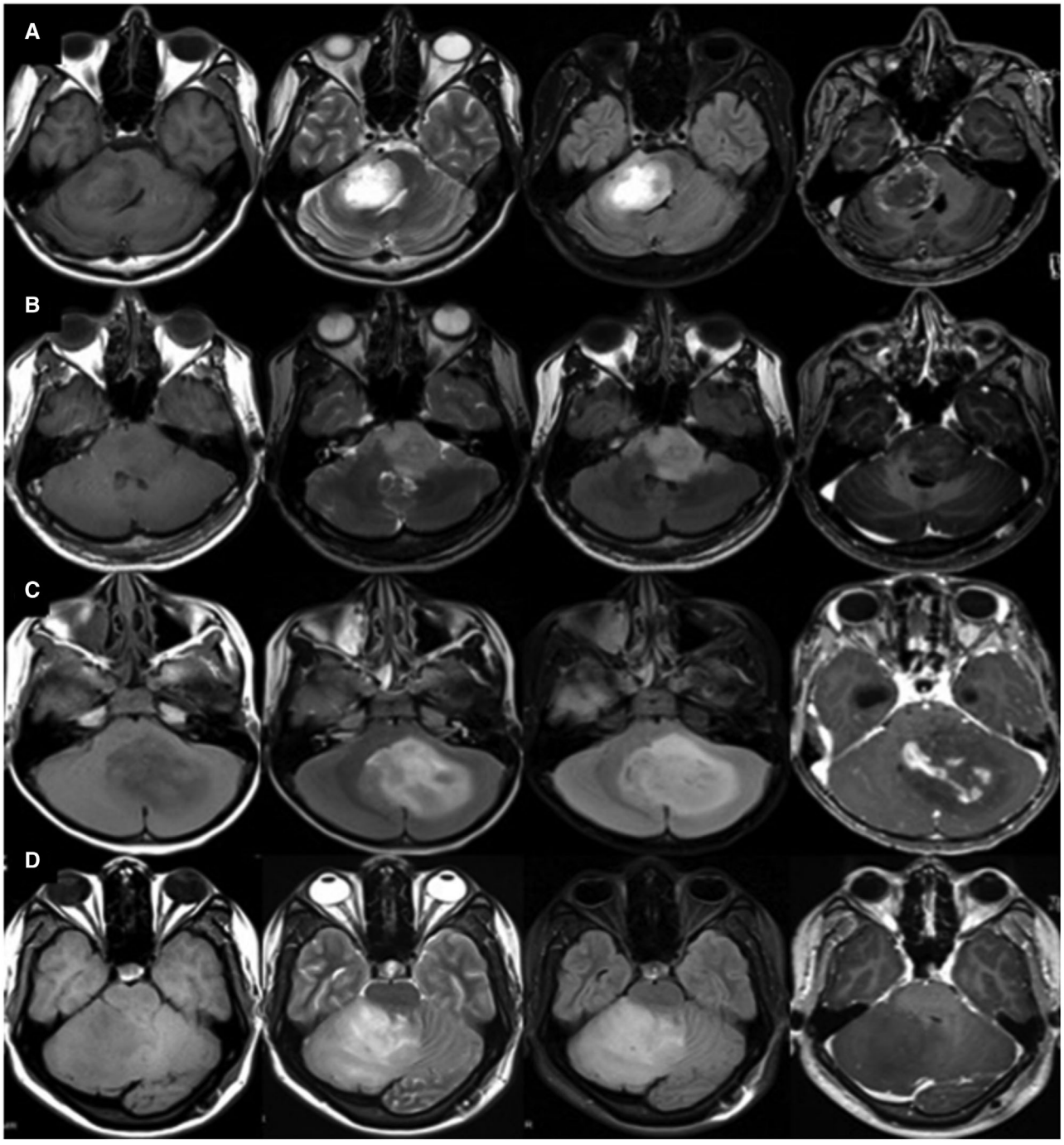

FIGURE 3 Examples of H3K27M-mutant and wild-type diffuse midline gliomas (DMGs) involving the middle cerebellar peduncle (MCP) and pons and cerebellum. A 17-year male with H3K27M-mutant (A, first row) DMG shows a well-defined, heterogeneous tumor involving right hemipons and MCP without edema and thick enhancing margin. A 34-year male with H3K27M wild-type DMG (B, second row) shows a poorly marginated tumor involving left hemipons and MCP with no associated edema and no post contrast enhancement. A 6-year female child with H3K27M-mutant (C, third row) DMG shows a well-marginated, mildly heterogeneous tumor involving left cerebellar hemisphere with no perilesional edema. There is patchy solid intense post contrast enhancement within the tumor. A 23-year male with H3K27M wild-type DMG (D, last row) shows a poorly marginated tumor involving right cerebellar hemisphere, mild perilesional associated edema, and no post contrast enhancement

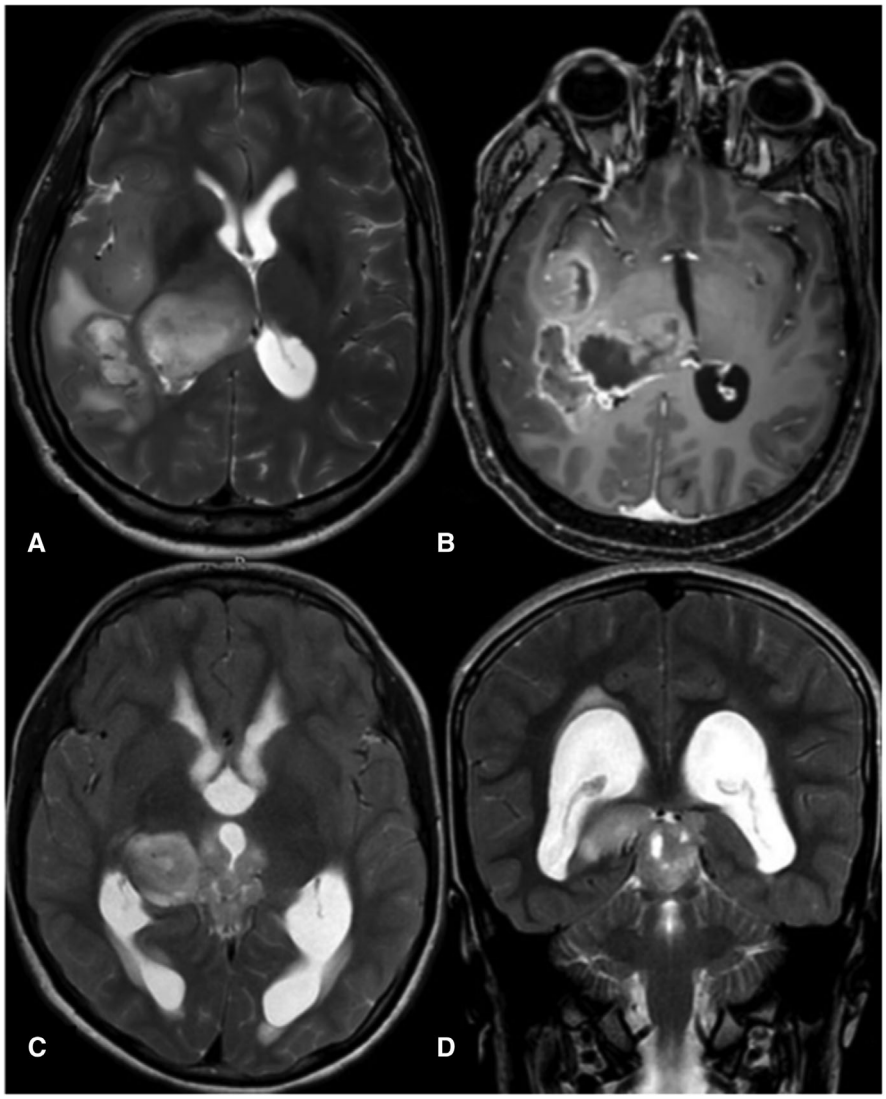

FIGURE 4 H3K27M wild-type right thalamic gliomas. A 38-year male with H3K27M wild-type right thalamic glioma (A and B, upper row). The lesion shows perilesional edema, cortical invasion, and thin post contrast rim enhancement. Another 18-year male patient with H3K27M-mutant (C and D, lower row) right thalamic glioma. The lesion shows well-defined margins, no significant perilesional edema, and exophytic component extending into the superior cerebellar cistern

compared to the WT gliomas (23.25%) ($p = 0.013$) (Figure 4). Brainstem tumors did not show any difference in terms of the presence of edema.

Twenty-seven (47.4%) of the mutant tumors showed ITSS grade 0, 1 (1.8%) ITSS grade 1, 2 (3.5%) ITSS grade 2, and 27% (47.4%) ITSS grade 3; whereas 25 (44.6%) WT tumors exhibited ITSS grade 0, 7 (12.5%) ITSS grade 1, 3 (5.4%) ITSS grade 2, and 21 (37.5%) showed ITSS grade 3. ITSS score was not found to be significantly different between mutant and WT DMGs ($p = 0.681$).

DISCUSSION

As per the decision of Working Committee 3 of the Consortium to Inform Molecular and Practical Approaches to CNS Tumor Taxonomy (cIMPACT-NOW), the term DMG, H3K27M-mutant should be earmarked for the diffuse tumors, that is, infiltrating, midline (e.g., involving the thalamus, brain stem, spinal cord, etc.), gliomas (astrocytic lineage), and H3K27M mutant, and must not be used for other tumors (as ependymoma or pilocytic astrocytoma) that possess H3K27M mutation.[16] H3K27M mutation is a gain-of-function mutation that modifies gene expression by posttranslational alterations in histone three, leading to altered DNA methylation and gliomagenesis via epigenetic regulation.[4] Genomic analysis of mutant DMGs has shown many correlated genetic variations, including mutations in the receptor tyrosine kinase/RAS/PI3K pathway, p53 overexpression, and ATRX (alpha-thalassemia/mental retardation syndrome X-linked) loss.[1,9]

In this study, approximately half of the midline located gliomas harbored the H3K27M mutation and were designated as DMG, H3K27M-mutant. Such incidence of the H3K27M mutation in midline gliomas

TABLE 2 The conventional imaging features of diffuse midline gliomas (DMG)

MRI features		Mutant, *n* (%)	Wild type, *n* (%)	*p*-value
Enhancement quality	None	9 (14.75)	20 (32.26)	0.032
	Minimal/mild	8 (13.11)	11 (17.74)	
	Marked/avid	44 (72.13)	31 (50)	
Thickness of enhancing margin	NA	9 (14.75)	20 (32.26)	0.050
	Thin/ <3 mm	23 (37.7)	13 (20.97)	
	Thick/ > 3 mm	9 (14.75)	6 (9.68)	
	Solid	20 (32.79)	23 (37.1)	
Definition of NCET margin	NA	0 (0)	2 (3.23)	0.001
	Well-defined	29 (47.54)	12 (19.35)	
	Equivocal	11 (18.03)	8 (12.9)	
	Poorly defined	21 (34.43)	40 (64.52)	
Proportion of edema	None/0	26 (42.62)	13 (20.97)	0.002
	<5%	23 (37.7)	18 (29.03)	
	6–33%	9 (14.75)	16 (25.81)	
	34–67%	3 (4.92)	15 (24.19)	
Cortical invasion	No	48 (78.69)	37 (59.68)	0.037
	Yes	13 (21.31)	25 (40.32)	
Heterogeneity	Homogeneous	11 (18.03)	16 (25.81)	0.07
	Mostly homogeneous	25 (40.98)	12 (19.35)	
	Mixed	14 (22.95)	17 (27.42)	
	Mostly heterogeneous	11 (18.03)	17 (27.42)	
Tumor margin	Ill-defined	18 (29.51)	29 (46.77)	0.074
	Well-defined	43 (70.49)	33 (53.23)	
Definition of CET margin	NA	9 (14.75)	20 (32.26)	0.073
	Well-defined	27 (44.26)	20 (32.26)	
	Equivocal	5 (8.2)	8 (12.9)	
	Ill-defined	20 (32.79)	14 (22.58)	

Note: The conventional imaging features of mutant and wild-type DMGs, irrespective of tumor grade and location, which showed significant difference (or tend to approach the level of significance).
Abbreviations: CET, contrast-enhancing tumor; *n*, number of patients; NA, not applicable; NECT, noncontrast-enhancing tumor.

has also been previously reported.[10,17,18] Mutant DMGs occur in the younger population as compared to WT DMGs.[10] In our study, the patients with mutated DMGs were approximately 12 years younger than WT DMG patients ($p = 0.016$). We did not find any significant difference in the gender distribution between the mutant and WT groups. The same has been observed earlier in the studies by Chen et al. and Schreck et al.[6,10]

We found that most of the DMGs (79%) were centered in the thalamus (with no significant difference between the groups). However, the difference was significant when brainstem location was considered, and a greater number of mutant DMGs were distributed in the brainstem than WT-DMGs. A similar finding has been reported by Schreck et al.[6] Over the past few years, the authors' institute's therapeutic strategy toward thalamic infiltrative neoplasms has included surgical resection, albeit subtotal in the majority of cases. This is predicated on the evidence accrued from recent literature for maximal surgical resection toward prolongation of the survival in thalamic high-grade gliomas.[19]

Our results revealed that certain cMRI features could be used to discriminate the H3K27M mutational status of DMGs. On intergroup and subgroup (brainstem and grade IV tumors) analyses, we found that the mutant gliomas demonstrated greater enhancement with thicker enhancing margins or solid enhancement as compared to the WT group. In comparison, the WT tumors exhibited more edema, poorly defined NCET margins, and more cortical invasion compared with the mutant DMGs. In the radiological evaluation results in the Radiotherapy in Paediatric and Adolescent Participants with High-Grade Glioma Phase II trial of nonbrainstem pediatric HGGs, the mutated DMGs have been reported to enhance avidly compared to WT DMGs.[20] The H3K27M mutation escalates the expression of growth

factors like platelet-derived growth factor and vascular endothelial growth factor by recurrent mutations and amplification of signaling genes like ACVR1, PI3K, and RTKs. The PIK3R1 mutations are reported to be obligatory to H3.3K27M mutations, and PIK3CA mutations are found in all DIPGs. These PIK3 mutations are the promoters of angiogenesis[21,22] that might account for the more florid enhancement of the mutant gliomas that we appreciated in this study. Contrast enhancement in H3K27M mutant paediatric midline gliomas has been earlier been reported in up to 67% of the cases in a study by Aboian et al.[23] The variation that we note in the present study likely arises from the varied age groups and locations of the tumors. In view of the limited extent of the literature on this subgroup of tumors, our observations on the proportions of enhancement of these lesions potentially add to the imaging spectrum of this newly classified tumor.

Histopathology literature is found wanting as to why mutant DMGs demonstrated a lesser degree of edema compared with the WT tumors. However, the same finding has also been discussed by Qiu et al. in their study of 66 patients with DMGs, where only 10 cases showed peritumoral edema.[24] Castel et al. have reported that the more aggressive H3.3 mutant DMGs exhibited lesser extracellular edema as compared to the less aggressive H3.1 mutant DMGs.[25] On the other hand, some authors found no significantly different cMRI parameters (such as tumor location, margin, cysts, necrosis, hemorrhage, degree, and pattern of contrast enhancement and edema) that could distinguish the mutant from WT DMGs.[2,6,10,25,26]

When we compared the cMRI features between thalamic mutant and WT tumors, mutant tumors showed more exophytic components. WT tumors showed significantly more edema; however, there was no difference in the enhancement and the definition of tumor margin between the two groups. The presence of exophytic growth pattern (tumor growing outside the borders of the structure of origin) confers a superior prognosis in brainstem gliomas than patients with tumors showing intrinsic growth patterns.[27–29] However, the same has not been described for the thalamic gliomas. This could indicate that the influence of this mutation in different anatomical locations may be variable, and these tumor subsets can be studied more comprehensively.

The limitations of this study include the lack of follow-up and no information regarding the survival data of the patients. Also, we did not perform any measurements to quantitate the degree of enhancement, which could increase the reproducibility of the results. Subgrouping of the histone of the H3.3/H3.1 gene group that could have been interesting was not performed in our study. Future studies with more extensive clinical data are needed to recognize various other aspects of H3K27M mutant DMGs, like outcome and management strategies, which are not discussed in this paper. Interscanner variability, although a potential confound in the imaging characteristics, is less likely to influence the results as the investigated variables were largely qualitative or semiquantitative.

To conclude, conventional MRI features, such as enhancement quality, the thickness of the enhancing margin, proportion of edema, definition of noncontrast-enhancing tumor margin, and cortical invasion can help discriminate between the H3K27M-mutant and WT DMGs. Among the varied imaging phenotypic characteristics of DMGs, these findings carry an important implication for treatment planning as well as designing future trials in this distinct group of neoplasms.

ACKNOWLEDGMENTS AND DISCLOSURE

The authors have no relevant financial or nonfinancial interests to disclose.

ORCID

Richa Singh Chauhan https://orcid.org/0000-0003-0919-1811
Karthik Kulanthaivelu https://orcid.org/0000-0002-1585-8769
Abhishek Kotwal https://orcid.org/0000-0003-4308-1704
Jitender Saini https://orcid.org/0000-0002-5218-0264

REFERENCES

1. Wang L, Li Z, Zhang M, et al. H3 K27M–mutant diffuse midline gliomas in different anatomical locations. Hum Pathol 2018;78:89-96.
2. Daoud EV, Rajaram V, Cai C, et al. Adult brainstem gliomas with H3K27M mutation: radiology, pathology, and prognosis. J Neuropathol Exp Neurol 2018;77:302-11.
3. Louis D, Perry A, Reifenberger G, et al. The 2016 World Health Organization Classification of Tumors of the Central Nervous System: a summary. Acta Neuropathol 2016;131:803-20.
4. Khuong-Quang DA, Buczkowicz P, Rakopoulos P, et al. K27M mutation in histone H3.3 defines clinically and biologically distinct subgroups of pediatric diffuse intrinsic pontine gliomas. Acta Neuropathol 2012;124:439-47.
5. Himes BT, Zhang L, Daniels DJ. Treatment strategies in diffuse midline gliomas with the H3K27M mutation: the role of convection-enhanced delivery in overcoming anatomic challenges. Front Oncol 2019;9:1-10.
6. Schreck KC, Ranjan S, Skorupan N, et al. Incidence and clinicopathologic features of H3 K27M mutations in adults with radiographically-determined midline gliomas. J Neurooncol 2019;143:87-93.
7. Johnson DR, Guerin JB, Giannini C, Morris JM, Eckel LJ, Kaufmann TJ. 2016 updates to the WHO Brain Tumor Classification System: what the radiologist needs to know. Radiographics 2017;37:2164-80.
8. Louis DN, Perry A, Reifenberger G, et al. The 2016 World Health Organization Classification of Tumors of the Central Nervous System: a summary. Acta Neuropathol 2016;131:803-20.
9. Solomon DA, Wood MD, Tihan T, et al. Diffuse midline gliomas with histone H3-K27M mutation: a series of 47 cases assessing the spectrum of morphologic variation and associated genetic alterations. Brain Pathol 2016;26:569-80.
10. Chen H, Hu W, He H, Yang Y, Wen G, Lv X. Noninvasive assessment of H3 K27M mutational status in diffuse midline gliomas by using apparent diffusion coefficient measurements. Eur J Radiol 2019;114:152-9.
11. Seong M, Kim ST, Noh JH, Kim YK, Kim HJ. Radiologic findings and the molecular expression profile of diffuse midline glioma H3 K27M mutant. Acta Radiol 2020;11:284185120968560 (Epub ahead of print).
12. Qon J. VASARI Research Project: The Cancer Imaging Archive (TCIA). Cancer Imaging Archive Wiki. Available at: www.wiki.cancerimagingarchive.net/display/Public/VASARI/Research/Project. Accessed March 20, 2021.
13. Zhou J, Reddy MV, Wilson BKJ, et al. MR imaging characteristics associate with tumor-associated macrophages in glioblastoma and provide an improved signature for survival prognostication. Am J Neuroradiol 2018;39:252-9.
14. Zhou H, Vallières M, Bai HX, et al. MRI features predict survival and molecular markers in diffuse lower-grade gliomas. Neuro Oncol 2017;19:862-70.

15. Park SM, Kim HS, Jahng GH, Ryu CW, Kim SY. Combination of high-resolution susceptibility-weighted imaging and the apparent diffusion coefficient: added value to brain tumour imaging and clinical feasibility of non-contrast MRI at 3 T. Br J Radiol 2010;83:466-75.
16. Louis DN, Giannini C, Capper D, et al. cIMPACT-NOW update 2: diagnostic clarifications for diffuse midline glioma, H3 K27M-mutant and diffuse astrocytoma/anaplastic astrocytoma, IDH-mutant. Acta Neuropathol 2018;135:639-42.
17. Feng J, Hao S, Pan C, et al. The H3.3 K27M mutation results in a poorer prognosis in brainstem gliomas than thalamic gliomas in adults. Hum Pathol 2015;46:1626-32.
18. Buczkowicz P, Bartels U, Bouffet E, Becher O, Hawkins C. Histopathological spectrum of paediatric diffuse intrinsic pontine glioma: diagnostic and therapeutic implications. Acta Neuropathol 2014;128:573-81.
19. Lim J, Park Y, Ahn JW et al. Maximal surgical resection and adjuvant surgical technique to prolong the survival of adult patients with thalamic glioblastoma. PLoS One 2021;16: e0244325.
20. Gutierrez DR, Jones C, Varlet P, et al. Radiological evaluation of newly diagnosed non-brainstem pediatric high-grade glioma in the herby phase II trial. Clin Cancer Res 2020;26:1856-65.
21. Duchatel RJ, Jackson ER, Alvaro F, Nixon B, Hondermarck H, Dun MD. Signal transduction in diffuse intrinsic pontine glioma. Proteomics 2019;19:e1800479.
22. Mazur M, Couldwell W. Investigating a candidate cell of origin for diffuse intrinsic pontine glioma. World Neurosurg 2011;76:368-9.
23. Aboian MS, Solomon DA, Felton E, et al. Imaging characteristics of pediatric diffuse midline gliomas with histone H3 K27M mutation. AJNR Am J Neuroradiol 2017;38:795-800.
24. Qiu T, Chanchotisatien A, Qin Z, Wu J, Du Z, Zhang X, Gong F, Yao Z, Chu S. Imaging characteristics of adult H3 K27M-mutant gliomas. J Neurosurg 2019;15:1-9.
25. Castel D, Philippe C, Calmon R, et al. Histone H3F3A and HIST1H3B K27M mutations define two subgroups of diffuse intrinsic pontine gliomas with different prognosis and phenotypes. Acta Neuropathol 2015;130:815-27.
26. Makepeace L, Scoggins M, Mitrea B, et al. MRI patterns of extrapontine lesion extension in diffuse intrinsic pontine gliomas. Am J Neuroradiol 2020;41:323-30.
27. Yoshikawa A, Nakada M, Watanabe T, et al. Progressive adult primary glioblastoma in the medulla oblongata with an unmethylated MGMT promoter and without an IDH mutation. Brain Tumor Pathol 2013;30:175-9.
28. Cohen ME, Duffner PK, Heffner RR, Lacey DJ, Brecher M. Prognostic factors in brainstem gliomas. Neurology 1986;36:602-5.
29. Horita Y, Wanibuchi M, Akiyama Y, et al. Exophytic glioblastoma multiforme originating from the medulla oblongata. Biomed Res Clin Pract 2016;1:58-61.

How to cite this article: Chauhan RS, Kulanthaivelu K, Kathrani N, et al. Prediction of H3K27M mutation status of diffuse midline gliomas using MRI features. J Neuroimaging. 2021;1-10. https://doi.org/10.1111/jon.12905